Journal of Hydrology 603 (2021) 127019

Contents lists available at ScienceDirect

Journal of Hydrology

journal homepage: www.elsevier.com/locate/jhydrol

# Moisture sources and paths associated with warm-season precipitation over the Sichuan Basin in southwestern China: Climatology and interannual variability

Sihan Zhang [a], Bo Liu [a,*], Guoyu Ren [a,b], Tianjun Zhou [c,d], Cong Jiang [e], Shangfeng Li [f], Baohuang Su [g]

[a] Department of Atmospheric Science, School of Environmental Studies, China University of Geosciences, Wuhan 430074, China
[b] Laboratory for Climate Studies, National Climate Center, China Meteorological Administration, Beijing, China
[c] State Key Laboratory of Numerical Modeling for Atmospheric Sciences and Geophysical Fluid Dynamics (LASG), Institute of Atmospheric Physics, Chinese Academy of Sciences, Beijing, China
[d] CAS Center for Excellence in Tibetan Plateau Earth Sciences, Chinese Academy of Sciences (CAS), Beijing, China
[e] School of Environmental Studies, China University of Geosciences, Wuhan 430074, China
[f] Jilin Provincial Key Laboratory of Changbai Mountain Meteorology and Climate Change, Laboratory of Research for Middle–High Latitude Circulation Systems and East Asian Monsoon, Institute of Meteorological Sciences of Jilin Province, Changchun, China
[g] State Key Laboratory of Severe Weather and Institute of Tibetan Plateau & Polar Meteorology, Chinese Academy of Meteorological Sciences, Beijing 100081, China

ARTICLE INFO

*Keywords:*
Warm-season precipitation
Sichuan Basin
Southwestern China
Interannual variability
HYSPLIT
Moisture pathways
Moisture sources

ABSTRACT

This study used the Hybrid Single-Particle Lagrangian Integrated Trajectory (HYSPLIT) model to examine the moisture sources and pathways associated with warm-season precipitation over the Sichuan Basin (SCB), southwestern China, with emphasis on the long-term mean state and interannual variability. Four groups of moisture pathways were identified over the period 1981–2017; i.e., the southwesterly, northeasterly, northwesterly, and westerly paths. With respect to the long-term mean state, the southwesterly path made the largest moisture contribution (36.0%) and, in combination with the northeasterly path (the importance of which has received little attention in previous studies), provided 70.2% of the total moisture. The Indian Ocean serves as the most important moisture source, accounting for 36.3% of the total moisture. In terms of interannual variability, compared with dry years, in wet years, the moisture contributions from the southwesterly path and the Indian Ocean increase by 18.6% (38.3% vs. 32.3%) and 20.71% (38.38% vs. 31.80%), but the contributions from the other moisture pathways and other major sources decrease. During the dry years, the northeasterly path, rather than the southwesterly path, provides the most moisture (34.6%). There are significant positive correlations between variations in runoff over the central and northern SCB and the moisture contribution from the Indian Ocean, which is associated with anomalous precipitation patterns over the SCB induced by fluctuations in the moisture contributions from the Indian Ocean.

## 1. Introduction

Lying in the upper reaches of the Yangtze River, the Sichuan Basin (SCB) is located to the east of the Tibetan Plateau and north of the Yunnan–Guizhou Plateau (Fig. 1) and has a high population density and prosperous economy. The SCB has a typical monsoon climate, and warm-season (May–September) rainfall accounts for >70% of the total annual precipitation (Li et al., 2016a). During the warm seasons over the period 1981–2017, 231 flooding events were recorded across China, causing losses in excess of $247 billion and affecting more than 2 billion people, and the SCB experienced 36.1% (83) of these events (Emergency Disasters Database: http://www.emdat.be/). Due to the complex terrain of the SCB, the heavy rainfall and frequent flooding often trigger geological hazards, such as debris flows and landslides, which have been responsible for a significant number of fatalities and other damage (Zhou et al., 2011). Moreover, the accumulated precipitation during the warm season shows obvious interannual variability, and during years with excessive precipitation the likelihood of flooding increases

* Corresponding author.
*E-mail address:* boliu@cug.edu.cn (B. Liu).

https://doi.org/10.1016/j.jhydrol.2021.127019

Available online 2 October 2021

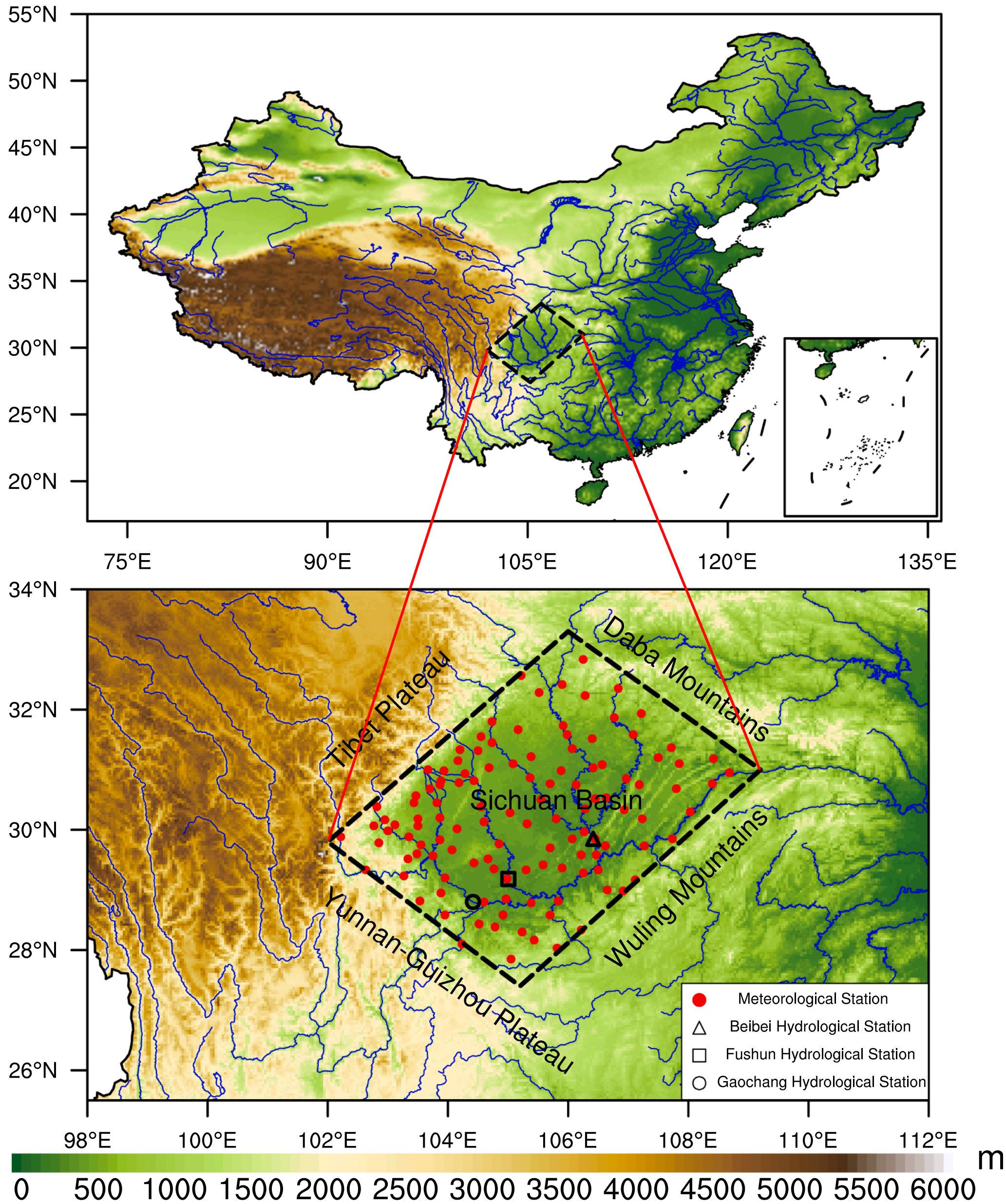


**Fig. 1.** Location of the Sichuan Basin (SCB). The shading represents the topography (units: m). Blue lines indicate rivers. (For interpretation of the references to colour in this figure legend, the reader is referred to the web version of this article.)

(Easterling et al., 2000; Jiang et al., 2017a). As pointed out by Xia et al. (2021), in years with above-average precipitation, several of the main tributaries that enter the SCB may suffer from floods simultaneously, which leads to tremendous flooding in the upper reaches of the Yangtze River. For example, in the middle of August 2020, precipitation amounts over the Mintuo and Jialing rivers in the SCB were 3.1 times and 2.8 times, respectively, more than the average (Xia et al., 2021), which resulted in economic losses of approximately $9.4 billion and affected 8.5 million people in southwestern China (Chinese Ministry of Emergency Management, https://www.mem.gov.cn/xw/yjglbgzdt/202101/t20210102_376288.shtml). Therefore, it is of vital importance to study the mechanisms involved in warm-season precipitation and its interannual variability over the SCB if we are to improve the prediction and mitigation of heavy rainfall and floods.

Generally, precipitation over a certain region is generated from local moisture already present in the atmosphere, local evaporation, and long-distance moisture transport (Brubaker et al., 1993). Among these sources, moisture transport from outside the region is essential for the generation of intense precipitation (Trenberth, 1999), which develops mostly during the warm season over southwestern China (Chen et al., 2021). In addition, local evaporation has potential impacts on precipitation formation by providing extra moisture and causing increased precipitation recycling (Pathak et al., 2014), whereas the contribution from the preexisting moisture is negligible. Within the framework of the Eulerian method, earlier studies have revealed the intrinsic relationship between precipitation and atmospheric moisture by analyzing the column integrated moisture flux. For the SCB, previous studies have found that warm-season precipitation is supplied by three moisture channels, and these are the southwesterly channel controlled by the Indian summer monsoon from the Bay of Bengal, the southeasterly channel controlled by the western Pacific subtropical high from the South China Sea and the western Pacific Ocean, and the westerly channel controlled by the mid-latitude westerlies from the Tibetan Plateau (Zhou et al., 2005; Jiang et al., 2007). Moreover, interannual variations in precipitation are influenced by moisture transport anomalies. The anomalous anticyclones over the western North Pacific and to the south of the

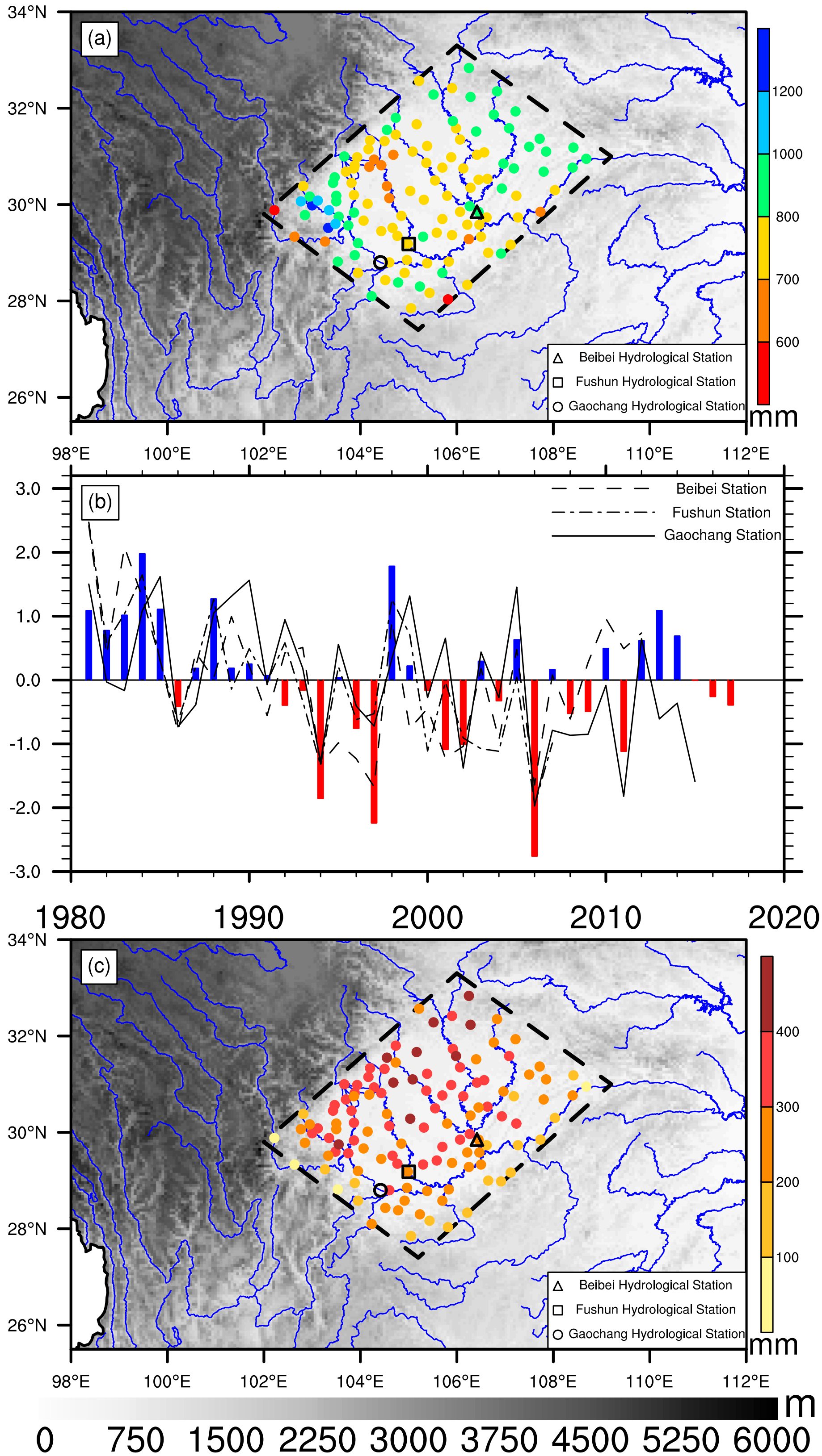


**Fig. 2.** (a) Spatial distribution of the mean warm-season accumulated precipitation (colored dots; units: mm). (b) Normalized time series of warm-season precipitation and river discharge. (c) Composite anomalies of warm-season precipitation (colored dots; units: mm) between wet and dry years.

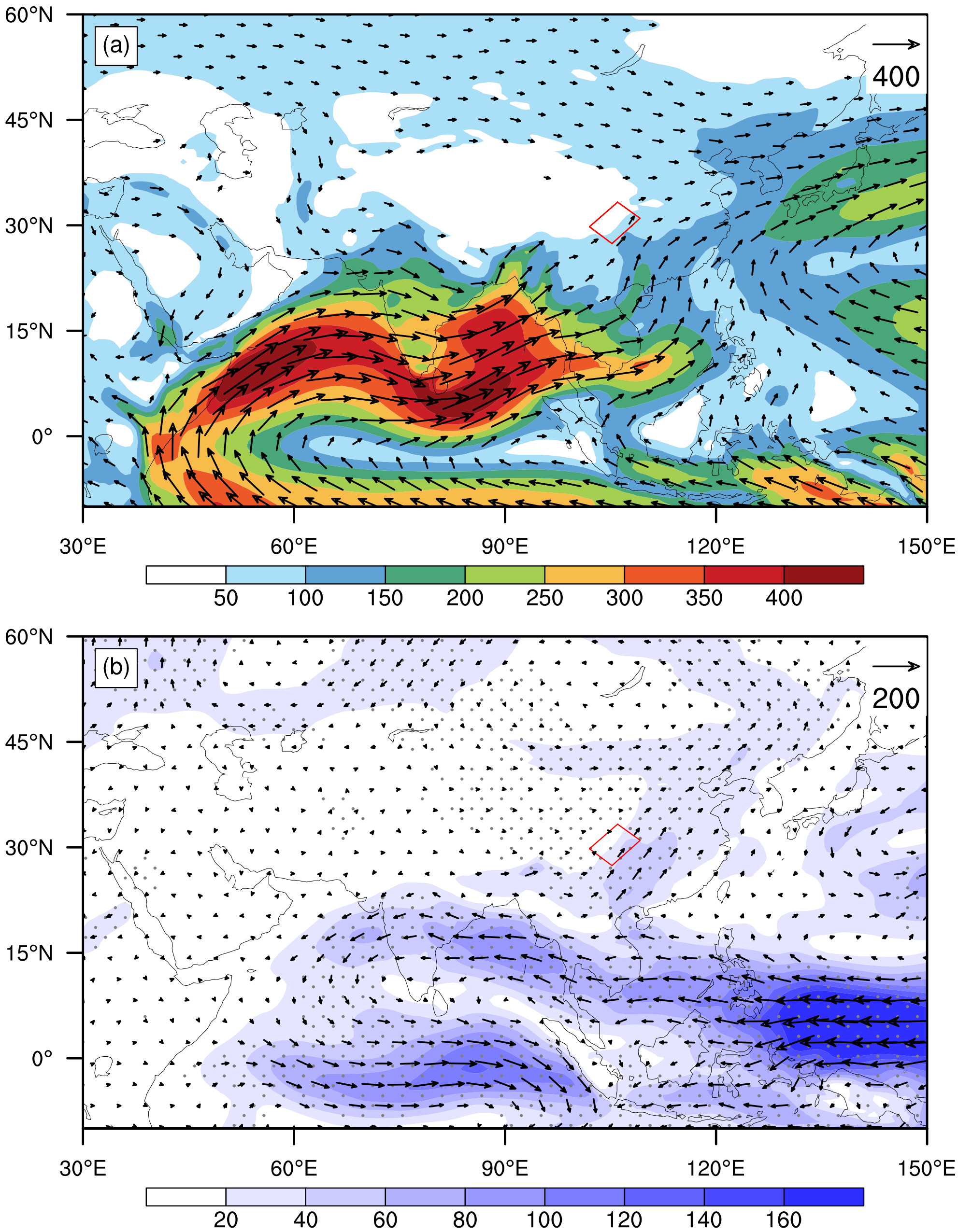


**Fig. 3.** (a) Climatology of the column-integrated moisture flux from the surface to 300 hPa (arrows; units: kg·m$^{-1}$·s$^{-1}$). Colored shading represents the amount of moisture flux. (b) Composite anomalies of the column-integrated moisture flux between wet and dry years. The red box indicates the target region (i.e., the Sichuan Basin; see Fig. 1). Dotted regions indicate the 95% confidence level based on Student's *t* test. (For interpretation of the references to colour in this figure legend, the reader is referred to the web version of this article.)

Tibetan Plateau strengthen moisture transport to the SCB, which favors excessive rainfall there (Jiang et al., 2017a).

The Eulerian approach has been proved to be effective in diagnosing moisture flows from and to a target precipitation region; however, it can hardly provide information on where the moisture originates from and which moisture sources are more important because of the quick shift of wind fields (Sodemann et al., 2008). To solve this problem, the Lagrangian method has been developed to identify the moisture pathways and to quantify the moisture contributions by generating trajectories along with specific humidity changes. Over recent decades, regional to global scale Lagrangian models ( Castillo et al., 2014; Nieto et al., 2019; Sun and Wang, 2014; Yang et al., 2020), including the Hybrid Single-Particle Lagrangian Integrated Trajectory model (HYSPLIT; Draxler and Hess, 1997, 1998), the Flexible Particle Dispersion model (FLEXPART; Stohl and James, 2004, 2005), and the Lagrangian analysis tool (LAGRANTO; Wernli and Davies 1997; Sprenger and Wernli 2015), have been widely used to quantify moisture sources and their contributions to individual or multiple rainfall events (Meseguer-Ruiz et al., 2020; Rapolaki, et al., 2020), as well as to examine the seasonal, interannual, and interdecadal variability of accumulated rainfall (Jiang et al., 2017b; Chu et al., 2019; Hu et al., 2021).

Huang and Cui (2015) analyzed the characteristics of the moisture transport associated with 70 heavy rainfall events over the SCB during the summers of 2009–2013 and found that the Indian Ocean makes the greatest contribution to extreme precipitation over the SCB. In addition, Chen and Xu (2016) studied the spatiotemporal structure of the moisture sources associated with 50 heavy (intense) precipitation events that occurred between 1980 and 2013 and found that the local and neighboring regions, together with the South China Sea, were the key moisture sources for these torrential rainfall events over the SCB. Until now, however, there have been few studies that used the Lagrangian method to study the climatology and interannual variability of moisture transport associated with precipitation over the SCB. Therefore, it is desirable to investigate the moisture sources and pathways that supply precipitation over the SCB in terms of the long-term mean state and interannual variability by using the Lagrangian method.

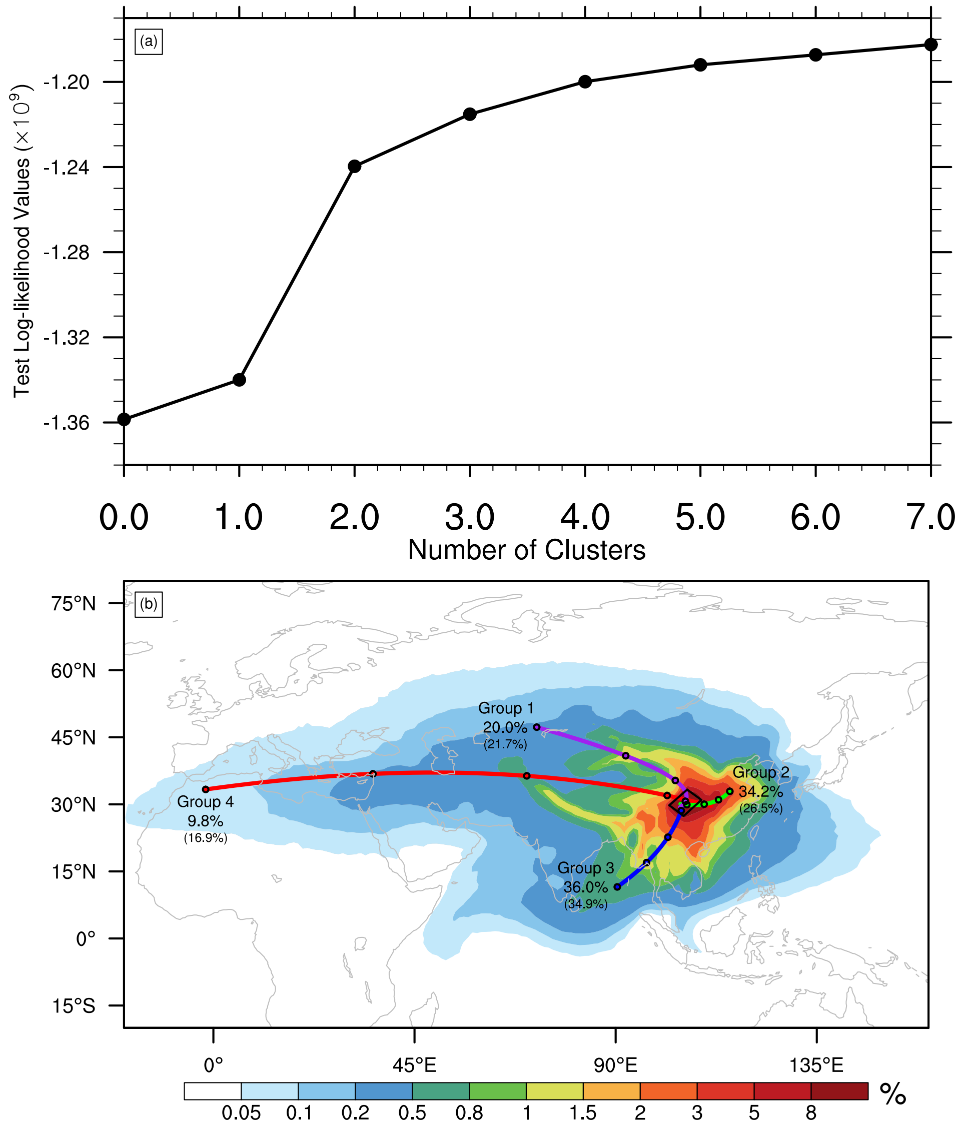


**Fig. 4.** (a) Different numbers of trajectory clusters corresponding to test log-likelihood values. (b) Four groups of clustered trajectories (bold lines) and the trajectory frequency (shading; units: %). The percentage trajectory frequency and moisture contribution made by each group is shown inside and outside the brackets, respectively.

The rest of this paper is organized as follows. Section 2 presents the data and methodology, including the configuration of the backward simulations. Section 3 shows the moisture sources and pathways associated with warm-season precipitation over the SCB for the climatological mean state and its interannual variability. Finally, a discussion and our concluding remarks are provided in Section 4.

## 2. Data and methodology

### 2.1. Observed and reanalysis datasets

We used observed daily precipitation data from the SCB recorded at 121 stations (red dots in Fig. 1) during the warm seasons (May to September) between 1981 and 2017. These data were obtained from the National Meteorological Information Center (NMIC) of the China Meteorological Administration (CMA). We also used daily runoff data from the main gauge stations at Beibei (controlling 156,736 $km^2$ and covering the period 1981–2012), Fushun (controlling 19,613 $km^2$ and covering the period 1981–2007), and Gaochang (controlling 135,378 $km^2$ and covering the period 1981–2015), which are situated on the Jialing, Tuo, and Min rivers, respectively (see Fig. 1). The 6-hr ERA-Interim reanalysis data (Dee et al., 2011) from 1981 to 2017, was used as the input data for the HYSPLIT model. This dataset has a horizontal resolution of 0.75° and 37 vertical pressure levels. The variables used included terrestrial height, geopotential height, zonal and meridional wind, vertical velocity, and specific humidity.

### 2.2. Backward simulations with HYSPLIT

We used the HYSPLIT model developed by the National Oceanic and Atmospheric Administration (NOAA) Air Resources Laboratory (ARL; Draxler and Hess, 1997, 1998) to calculate the air parcel trajectories. This model has been extensively used to track and forecast the release of radionuclides, wildfire smoke, windblown dust, air pollution, and moisture (e.g., Tichý et al., 2017; Chen and Luo, 2018; Kalabokas et al., 2020; Kim et al., 2020; Yang et al., 2021).

In the model of the backwards trajectory, the air parcel is set to move with the wind. The movement of the air parcel is the integral of its position vector through space and time. The final position of the air parcel $P(t+\Delta t)$ is calculated as the average velocity between the initial position $P(t)$ and the first guess position $P'(t+\Delta t)$. The first guess position is written as:

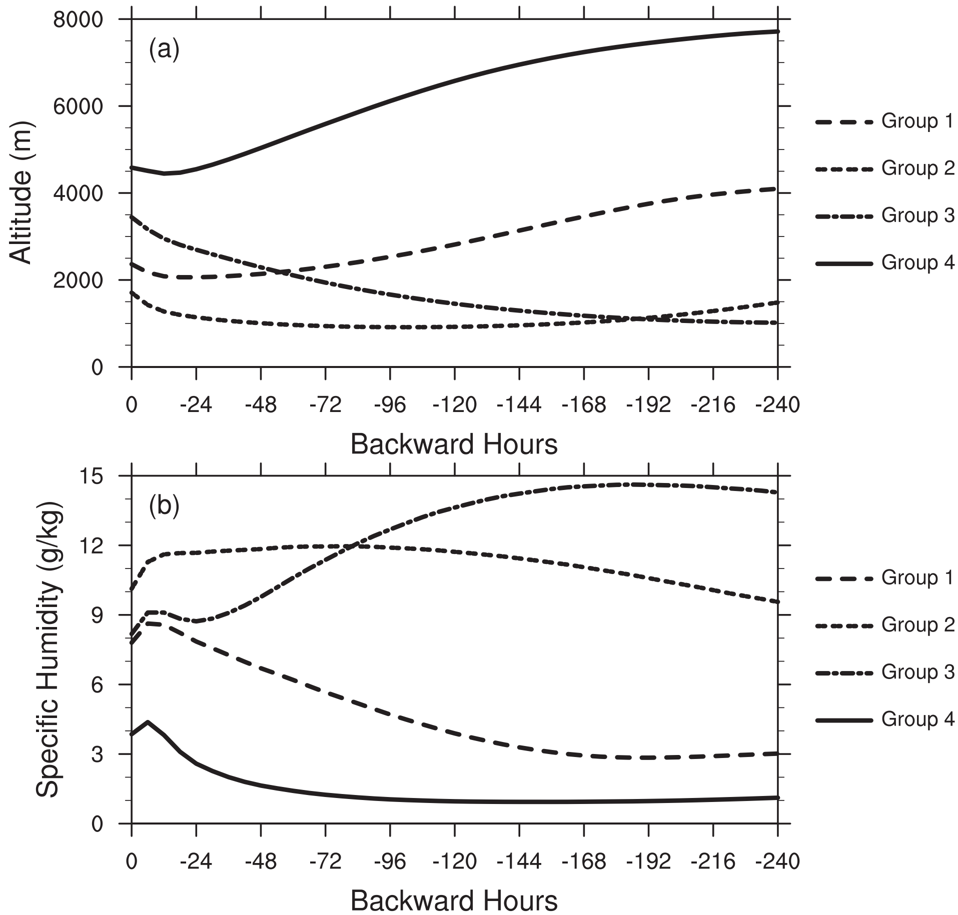


**Fig. 5.** Averaged (a) altitude and (b) specific humidity along the four groups of trajectories from 10 days prior (−240 hr) to the moment that the air parcel reached the target region (0 hr).

$$P^{'}(t+\Delta t) = P(t) + V(P,t)\Delta t. \quad (1)$$

The final position is expressed as:

$$P(t+\Delta t) = P(t) + 0.5 \times (V(P,t) + V(P^{'}, t+\Delta t))\Delta t, \quad (2)$$

where $\Delta t$ is the time step (6 hr in this study).

We used the HYSPLIT model to simulate the backward trajectories. The target region was the SCB, as illustrated by the area inside the box in Fig. 1, and the simulations were carried out every 6 hr during the warm season (May to September) from 1981 to 2017. The air parcels were released from the objective region at five above-ground levels (AGL) of 500, 1500, 3000, 5000, and 9000 m, and 510 horizontal locations with a resolution of 0.5°. In this way, we obtained 11,548,440 backward trajectories. Each backward simulation lasted for 10 days (240 hr), which is considered to be the retention time of moisture in the atmosphere (Eagleson, 1970; Trenberth, 1998). The output of the HYSPLIT model was recorded at 6-hr intervals and included the three-dimensional position (latitude, longitude, and AGL) and specific humidity of the air parcels.

### 2.3. Clustering of backward trajectories

To identify the main moisture paths from the large number of backward trajectories, we applied a clustering method using the Curve Clustering Toolbox (Gaffney, 2004), which has been used in several previous studies (e.g., Li et al., 2016b; Chen and Luo, 2018; Rapolaki et al., 2020). In the clustering procedure, the different number of clusters (k) have a corresponding in-sample log-likelihood value, which is a goodness-of-fit metric for probabilistic models and is expressed as the log-probability of the observed data (see Gaffney, 2004 for details).

### 2.4. Calculation of moisture contribution

To obtain a better understanding of moisture transport associated with precipitation over the SCB, we quantified the moisture contributions from different clusters of trajectories as well as from the individual moisture sources. Each air parcel tracked can undergo multiple cycles of moisture uptake (evaporation) and loss (precipitation) before arriving in the target region (i.e., the SCB). The changes in the moisture content for an air parcel can be expressed as "evaporation minus precipitation" (Stohl and James, 2004, 2005):

$$e_a - p_a = m\frac{\Delta q_a}{\Delta t}, \quad (3)$$

$$\Delta q_a = q_a - q_{a-\Delta t}, \quad (4)$$

where $e_a$ and $p_a$ are the rates of moisture uptake (evaporation) and loss (precipitation), respectively, along the trajectory at time $a$, and $m$ is the mass of the air parcels. $\Delta t$ is the time step of the backward tracking (6 hr in this study), and $\Delta q_a$ represents the changes in specific humidity $q$ from time $a-\Delta t$ to $a$. That is, when $\Delta q_a > 0$, the moisture content of the air parcel increases at time $a$ since evaporation gain is larger than precipitation loss, and vice versa.

#### 2.4.1. Moisture contribution of each cluster

The moisture contribution ratio of the cluster $c$ to the total moisture released over the target area $CR(c)$ can be expressed as follows:

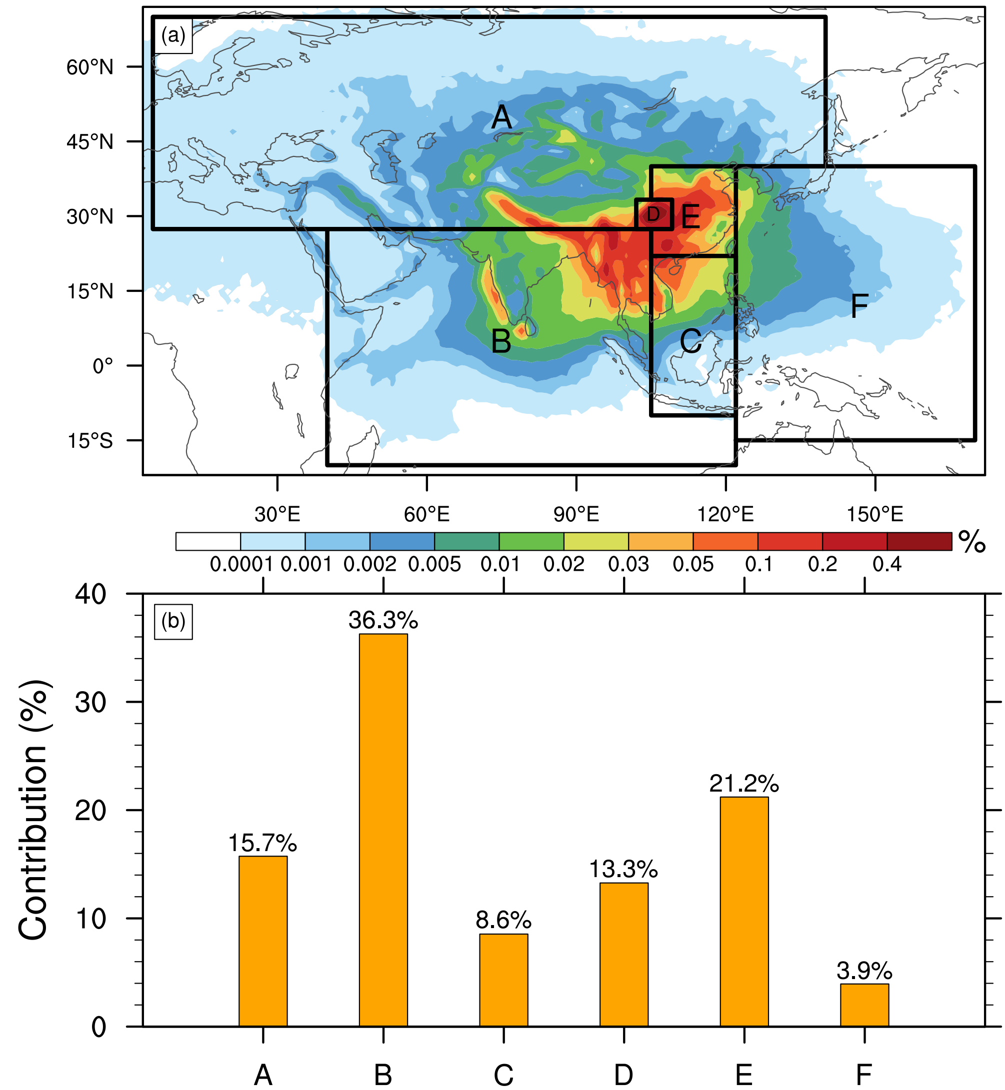


**Fig. 6.** (a) Spatial distribution of moisture contribution (shading; units: %) to the target region. (b) Moisture contribution (units: %) from different moisture sources to precipitation. The number above each column represents the percentage contribution from the corresponding region. Regions A–F represent Eurasia, the Indian Ocean, the South China Sea, the Sichuan Basin, eastern China, and the western North Pacific, respectively.

$$CR(c) = \frac{\sum_1^m \Delta q_{t=-6}}{\sum_1^n \Delta q_{t=-6}} \times 100\%, \tag{5}$$

where $\Delta q_{t=-6}$ is the change in specific humidity $q$ of a trajectory from time $t = -6$ to $t = 0$. $m$ is the number of trajectories in the cluster $c$, and $n$ is the total number of trajectories.

### 2.4.2. *Moisture contribution from each source*

Considering the multiple cycles of evaporation gain and precipitation loss of each air parcel, Sodemann et al. (2008) developed a comprehensive "source attribution method", which has been widely used (e.g., Sun and Wang, 2015; Chen and Luo, 2018; Peng et al. 2020) to quantify the moisture contribution from each grid area. The effective specific humidity change of air parcels at time $a$ to the target area $Q_a$ is used to calculate the moisture contribution from each grid area to the precipitation in the study region. The details of this approach are as follows.

1) If evaporation is less than or equal to precipitation ($e_a - p_a \leqslant 0$) for the air parcel at time $a$, $Q_a$ is set to 0.
2) When $e_a - p_a > 0$, $Q_a$ is set temporarily to $\Delta q_a$. To calculate the final $Q_a$, $\Delta q_b$ should be considered in the calculation and time $b$ is any time after time $a$ (excluding the last 6 hr before reaching the study area). If $\Delta q_b \geqslant 0$ is maintained, $Q_a$ equals to $\Delta q_a$. If $\Delta q_b < 0$, $Q_a$ is decreasing by the following proportion,

$$Q_a = \Delta q_a \times \frac{q_{b-\Delta t}}{q_b}, \tag{6}$$

where $q_{b-\Delta t}$ and $q_b$ are the specific humidity of air parcels at time $b - \Delta t$ and time $b$, respectively.

3) The effective moisture contribution ratio of region $i$ to the target area $CR(i)$ can be expressed as follows:

$$CR(i) = \frac{\sum Q(i)}{\sum q_{t=-6}} \times 100\%, \tag{7}$$

where $\sum Q(i)$ is the sum of the effective specific humidity change for all air parcels over the region $i$, while $\sum q_{t=-6}$ is the total specific humidity of all air parcels over the last 6 hr before reaching the target region.

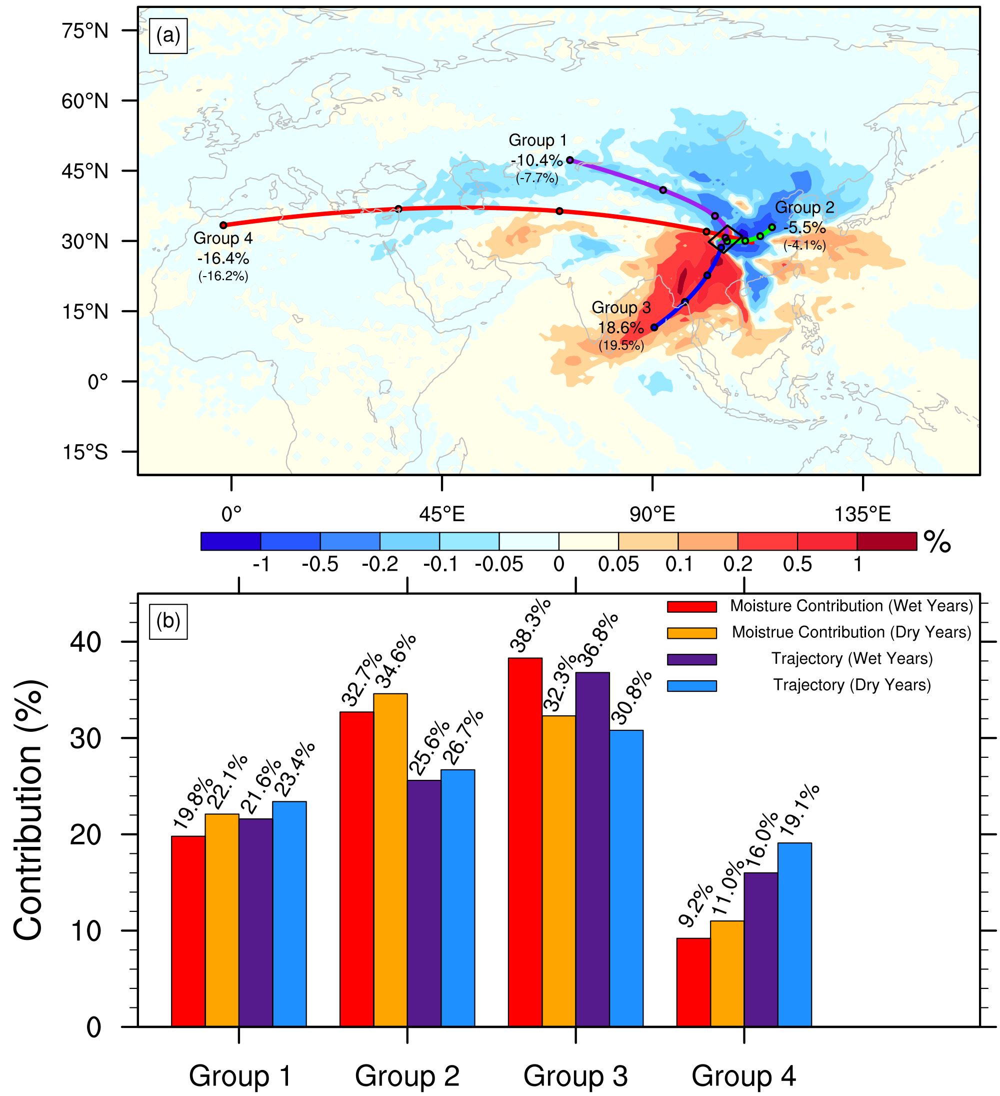


**Fig. 7.** (a) Four groups of clustered trajectories (bold lines) and composite differences of trajectory frequency (shading; units: %) between wet and dry years. The percentages of the relative trajectory frequency difference and the relative moisture contribution difference for each group are indicated inside and outside the brackets. (b) Moisture contribution and trajectory frequency (units: %) of each group in wet and dry years.

## 3. Results

### 3.1. Warm-season rainfall over the SCB and the associated moisture transport

Fig. 2a shows the spatial distribution of the mean warm-season precipitation over the period 1981–2017. Overall, averaged over the SCB, the mean total warm-season precipitation was 806.7 mm, with centers of maximum rainfall located over the western SCB, such as at Ya'an (29°59′N, 103°00′E), Leshan (29°34′N, 103°45′E), and Meishan (30°04′N, 103°48′E), where the total precipitation exceeded 1200 mm. These features are generally consistent with previous studies (Zhu and Yu, 2003). Moreover, the warm-season precipitation over the SCB is characterized by significant interannual variability, as indicated by the normalized time series of warm-season precipitation averaged at 121 meteorological stations over the SCB during the period 1981–2017 (Fig. 2b), where a positive (negative) value represents adequate (inadequate) rainfall. In addition, we found significant positive correlations between the total warm-season precipitation over the SCB and total runoff from the rivers Jialing ($R = 0.75$, $p < 0.01$), Tuo ($R = 0.76$, $p < 0.01$), and Min ($R = 0.61$, $p < 0.01$; Fig. 2b), suggesting that flooding is closely related to warm-season precipitation over interannual timescales. Based on the normalized precipitation values above 1 or below 1 standard deviations, we classified six years with maximum above-normal values as wet years (1981, 1984, 1985, 1988, 1998, and 2013), and six years with minimum below-normal values as dry years (1994, 1997, 2001, 2002, 2006, and 2011). During the wet years, increases in warm-season precipitation were recorded consistently at all stations over the SCB, but increases of more than 400 mm relative to the dry years occurred mostly in the central and northern parts of the SCB (Fig. 2c).

The climatology of the column-integrated atmospheric water vapor flux between May and September is shown in Fig. 3a. The primary moisture channel supplying precipitation over the SCB was the southwest channel from the Indian Ocean and the Indochina Peninsula. The moisture fluxes delivered by both the south (from the Maritime Continent) and southeast (from the western North Pacific) channels were relatively weaker. These features are similar to those described in previous studies (Zhou et al., 2005; Huang and Cui, 2015; Chen and Xu, 2016). Compared with dry years, the southwesterly wind anomalies from the Yunnan–Guizhou Plateau significantly enhance moisture transport to the SCB in wet years, as reported by Jiang et al. (2007) and Li et al. (2010), which is favorable for rainfall over the SCB (Fig. 3b).

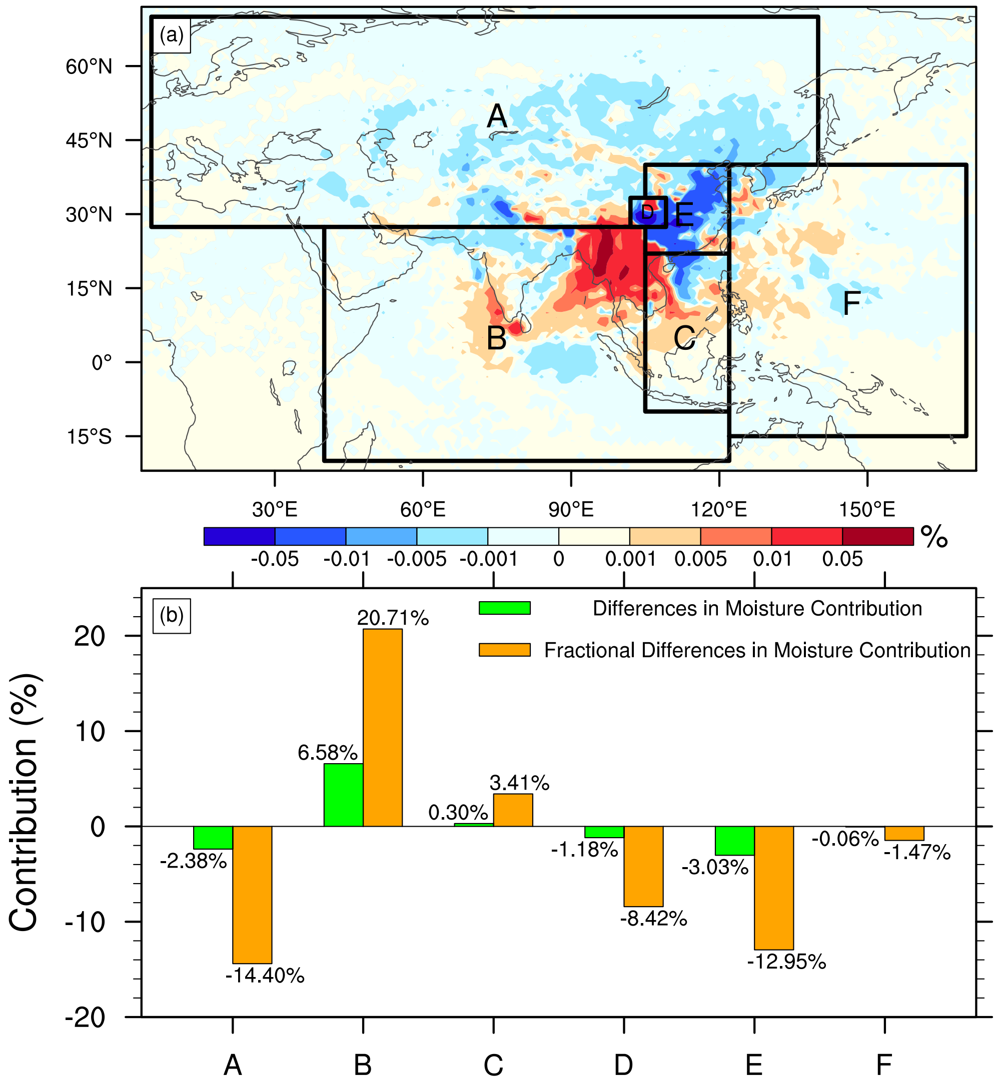


**Fig. 8.** (a) Composite differences of moisture contribution (shading; units: %) to the target region between wet and dry years. (b) Moisture contribution differences and fractional differences in moisture contribution (units: %) from different moisture sources to precipitation between wet and dry years. Regions A–F represent Eurasia, the Indian Ocean, the South China Sea, the Sichuan Basin, eastern China, and the western North Pacific, respectively.

### *3.2. Climatology of moisture sources and paths*

To investigate the sources and paths associated with the moisture supply for warm-season precipitation over the SCB, we used the concept of "effective trajectory", which is defined with a decrease in specific humidity during the last 6 hr before arrival in the target region (i.e., the SCB). By definition, the effective trajectories are those that contribute to rainfall over the SCB. We identified 3,922,028 effective trajectories, which accounted for 34.0% of all trajectories. We divided these trajectories into four groups using the clustering method outlined above. The curve in Fig. 4a shows diminishing returns in terms of improvement in fit beyond $k = 4$; consequently, this is a reasonable endpoint for the cluster analysis, and hence the number of clusters that we used for the moisture trajectories was 4.

Fig. 4b shows the distribution of the trajectory frequency and the four groups of moisture pathways for the SCB between May and September. Black circles represent the mean position of the air parcels in each group of backward trajectories on the first (−24 hr), fourth (−96 hr), seventh (−168 hr), and tenth (−240 hr) day before the precipitation. Overall, the four groups of pathways coincide with the high values of the trajectory frequency. The average altitude and specific humidity within each group along the pathways during the 10 days of backward tracking are shown in Fig. 5. During the last 6 hr, the altitude of the four group-mean trajectories rises and the specific humidity decreases, indicating intense moisture condensation with a strong ascending motion.

Among all groups, the southwesterly path (Group 3) from the Bay of Bengal was the most important moisture transport pathway, accounting for 36.0% of the total moisture and 34.9% of the total trajectories. This group of pathways is ocean-originated and during the early period of the simulation (−240 to − 96 hr; "−" indicates the "backward" simulation) it had the highest specific humidity (Fig. 5). As it moved to the target region, the altitude (specific humidity) increased (decreased) until about −24 hr, indicating a large amount of moisture loss due to the influence of the topography along the pathways, such as the Indochina Peninsula and the Yunnan–Guizhou Plateau. Furthermore, it experienced moisture uptake over the SCB during the last day before arriving at the target region (Fig. 4b and 5). The northeasterly path (Group 2) ranked second in both trajectory contribution (34.2%) and moisture contribution (26.5%). However, the importance of this group of pathways has rarely been stressed in previous studies. Along this path, the air parcels maintained a high specific humidity (over 9 g $kg^{-1}$) and a low altitude (below 2000 m), with no large variability until the last 12 hr before reaching the target region (Fig. 5). The remaining two groups of

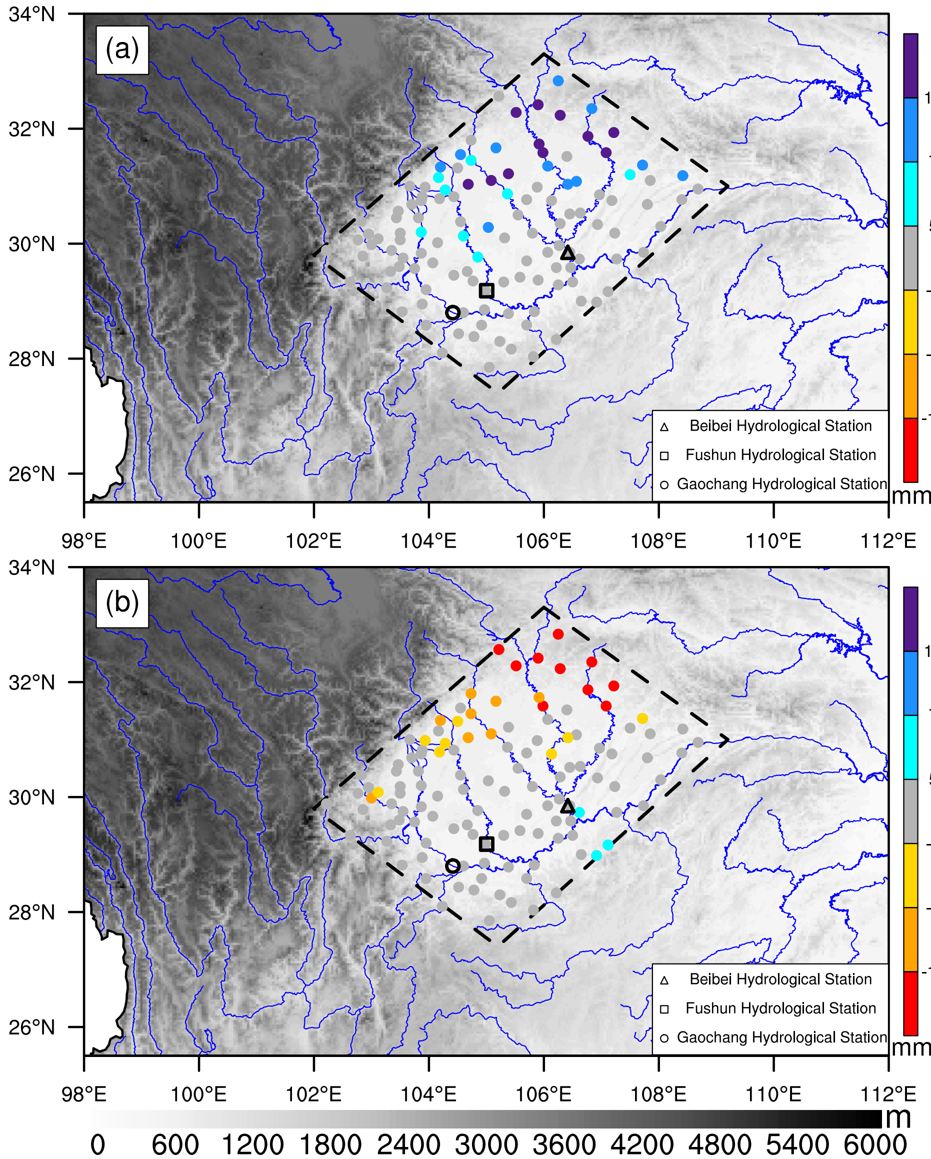


**Fig. 9.** Patterns of linear regression of precipitation at each station (colored dots; units: mm) onto interannual variations in moisture contributions from (a) the Indian Ocean and (b) the Sichuan Basin.

pathways; i.e., the northwesterly (Group 1) and westerly (Group 4) paths, together contributed less than a third (~29.8%) of the total moisture. The altitude (specific humidity) was among the highest (lowest) of the four paths almost throughout the pathway, especially the trajectories in Group 4, for which the specific humidity was always < 5 g kg$^{-1}$. The moisture uptake for both of these groups occurred mainly near the Qinghai–Tibet Plateau and the SCB within the last 4 days (−96 to − 6 hr; Fig.s 4b and 5).

Fig. 6a shows the spatial distribution of the moisture contribution to warm-season precipitation over the SCB, which is similar to that of the trajectory frequency in Fig. 4b, and the differences can be attributed mainly to changes in specific humidity along the trajectories. For instance, the moisture contributions from the western Arabian Sea (>0.02% over most regions) and the western Indian Peninsula (<0.001% over most regions) are in sharp contrast, and this can be attributed largely to the orographic precipitation caused by the Western Ghat over the western Indian Peninsula. To identify the major moisture sources and their contributions, we calculated the contributions from six moisture source regions, as illustrated in Fig. 6a, namely, Eurasia (A), the Indian Ocean (B), the South China Sea (C), the Sichuan Basin (D), eastern China (E), and the western North Pacific (F). The moisture contributions from the individual regions on climatological state are shown in Fig. 6b. The Indian Ocean (B) is the most important moisture source, accounting for 36.3% of the total moisture contribution. High moisture contributions occur in the Bay of Bengal and Indochina Peninsula over the Indian Ocean region. Eastern China (E) and Eurasia (A) make important moisture contributions to the target region, supplying 21.2% and 15.7%, respectively. For Eurasia, high values are found over the Qinghai–Tibet Plateau, especially to its south. In addition, the Sichuan Basin (D) contributes 13.3% of the moisture, indicating that evaporation over the SCB contributes to warm-season precipitation within the region itself. The South China Sea (C) and western North Pacific (F) contribute the least moisture to rainfall over the SCB, and account for only 8.6% and 3.9%, respectively, of the moisture contribution to the target region.

### 3.3. Interannual variability of moisture sources and paths

Fig. 7 shows the differences in trajectory frequency and the four groups of moisture channels between wet and dry years. Compared with

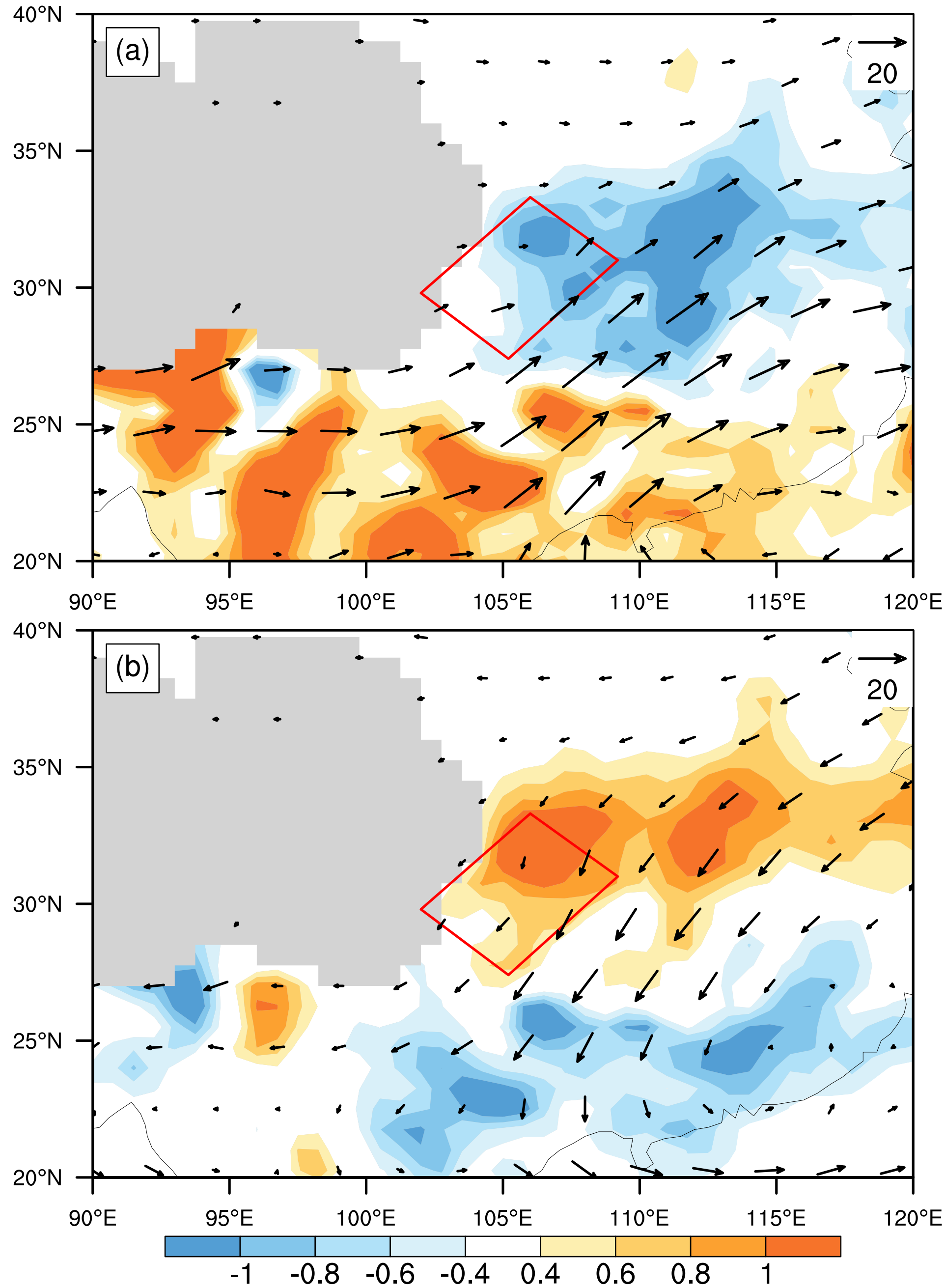


**Fig. 10.** Linear regression of column-integrated moisture flux from surface to 300 hPa (arrows; units: $kg \cdot m^{-1} \cdot s^{-1}$) and its divergence (colored shading; units: $10^{-5} \times kg \cdot m^{-2} \cdot s^{-1}$) onto interannual variations in the moisture contributions from (a) the Indian Ocean and (b) the Sichuan Basin.

dry years, the wet years show a significant increase in the frequency of southwesterly trajectories across the Bay of Bengal and Indochina Peninsula, whereas there is a decrease in the frequency of northeasterly trajectories across eastern and northern China. For the southwesterly path (Group 3) from the Bay of Bengal, in wet years, the corresponding moisture contribution and trajectory frequency increase by 18.6% (38.3% vs. 32.3%) and 19.5% (36.8% vs. 30.8%), respectively, over the dry years. In contrast, the moisture contributions (trajectory frequencies) of the westerly path (Group 4), the northwesterly path (Group 1), and the northeasterly path (Group 2) decreased by 16.4% (16.2%), 10.4% (7.7%), and 5.5% (4.1%), respectively. However, in contrast to the long-term mean state, during the dry years the northeasterly path (Group 2), instead of the southwesterly path (Group3), becomes the most important path in terms of moisture contribution (34.6%; Fig. 7b), which indicates the potential impacts of the northeasterly path on regulating warm-season precipitation over the SCB.

The composite differences in moisture contribution to the target region and the moisture contribution differences of the six source regions between wet and dry years are shown in Fig. 8. The spatial distribution of moisture contribution changes is mostly consistent with that of the trajectory frequency changes, indicating that an increase in trajectory frequency may lead to an increased moisture contribution from a certain region. Compared with dry years, during the wet years, moisture contribution from the Indian Ocean (B) increases by 20.71% (38.38% vs 31.80%), and especially significantly from the Bay of Bengal and Indochina Peninsula. Consistent with the composite analysis, there is a significant positive correlation ($R = 0.53$, $p < 0.01$) between the time series of total warm-season precipitation and the moisture contribution from the Indian Ocean (B). In contrast, the moisture contributions from eastern China (E), Eurasia (A), and the Sichuan Basin (D) decrease by

12.95% (20.38% vs. 23.41%), 14.40% (14.17% vs. 16.56%), and 8.42% (12.87% vs. 14.05%), respectively. In addition, compared with the above sources, the changes in moisture contributions from the South China Sea (C) and western North Pacific (F) are almost negligible.

Furthermore, the interannual variability of runoff across the SCB can be linked to changes in the moisture contributions from the various sources. For example, variations in runoff from the Jialing River ($R = 0.51$, $p < 0.05$) and the Tuo River ($R = 0.44$, $p < 0.05$) are closely correlated with moisture contribution from the Indian Ocean. This is because when moisture contributions from the Indian Ocean are higher than normal, excess warm-season precipitation is observed over the central and northern SCB, where the Jialing and Tuo basins are located (Fig. 9a). In contrast, variations in runoff from the Jialing are significantly negatively correlated ($R = -0.53$, $p < 0.05$) with the moisture contribution from the SCB because when the moisture contribution from the SCB increases, negative precipitation anomalies occur over the Jialing Basin (Fig. 9b). However, variations in moisture contributions from the other four sources are poorly correlated with runoff across the SCB.

To investigate the possible mechanisms behind the relationship between moisture contributions and the precipitation anomalies, we regressed the column-integrated moisture flux and the associated divergence onto the variations in moisture contributions from two sources; i.e., the Indian Ocean and SCB. In years with an above-normal moisture contribution from the Indian Ocean, significant moisture convergence anomalies occur over central and northern parts of the SCB associated with the increase in moisture transport from the Indian Ocean (Fig. 10a). This leads to an increase in local precipitation (Fig. 9a) and increased runoff from the rivers Jialing and Tuo. In contrast, in years with an above-normal moisture contribution from the Sichuan Basin, there are significant moisture divergence anomalies over central and northern parts of the SCB. This leads to a reduction in moisture transport from the Indian Ocean (Fig. 10b), which significantly suppresses precipitation (Fig. 9b) and reduces runoff from the Jialing River.

## 4. Discussion and conclusions

In this study, climatological moisture sources and pathways, and their interannual variability, associated with precipitation across the Sichuan Basin (SCB) during the warm season (May to September) over the period 1981–2017 were investigated using the HYSPLIT model. Our main findings are summarized below.

For the long-term mean state over the period 1981–2017, the trajectories were clustered into four groups: the southwesterly, northeasterly, northwesterly, and westerly paths. The southwesterly path from the Indian Ocean was the most important path and accounted for 34.9% of total trajectories and 36.0% of total moisture. The northeasterly path, across eastern China, ranked second in both trajectory contribution (26.5%) and moisture contribution (34.2%). These two pathways combined to contribute more than 70% of all moisture. Regarding the moisture contribution from individual sources, the Indian Ocean, accounting for 36.3% of all moisture, was the most important moisture source for precipitation over the SCB. In addition, eastern China (21.2%), Eurasia (15.7%), and the Sichuan Basin (13.3%) also served as important moisture contributors.

Regarding the interannual variability, compared with dry years, there were significant increases during wet years in the moisture contributions from the southwesterly path of 18.6% (38.3% vs. 32.3%) and the Indian Ocean of 20.71% (38.38% vs. 31.80%). In contrast, the contributions from the other moisture pathways and major source areas were lower in the wet years than in the dry years. In the wet years, the southwesterly path ranked first for moisture contribution (38.3%), whereas in the dry years, the northeasterly path was most important (34.6%). Furthermore, the yearly moisture contribution from the Indian Ocean was significantly positively correlated ($R = 0.53$, $p < 0.01$) with total warm-season precipitation over the SCB.

Further analysis revealed significant correlations between the variations in moisture contributions from the various sources and the fluctuations in runoff across the SCB over interannual timescales. A significant positive correlation was found between moisture contributions from the Indian Ocean and runoff from the Jialing River ($R = 0.51$, $p < 0.05$) and the Tuo River ($R = 0.44$, $p < 0.05$), which we interpreted as being related to the anomalous precipitation over the Jialing and Tuo basins associated with the variations in moisture contributions from the Indian Ocean. In contrast, we found a significant negative correlation ($R = -0.53$, $p < 0.05$) between moisture contributions from the SCB and runoff from the Jialing River, which we relate to anomalous precipitation over the Jialing Basin associated with variations in moisture contributions from the SCB.

It should be mentioned that not all moisture can be attributed by using the “moisture source attribution method” (Sodemann et al., 2008). One reason for this is the residence time of moisture in the atmosphere used for this study was 10 days. It is known that the longer the backward tracking time, the more moisture can be identified for precipitation over the target region. However, when the backward tracking time is beyond 10 days, wind field errors can lead to large deviations of trajectories (Stohl and Seibert, 1998). The other is that 10 days before reaching the target area, the air parcels are not assured to have a zero specific humidity, and this part of the moisture is not attributed. For this study, the attributable moisture accounted for about 70.0%, 68.5%, and 70.0% of all moisture for the long-term mean state of the period 1981–2017, the selected wet years, and the selected dry years, respectively, which is similar to the values reported in previous studies (Sodemann and Zubler, 2009; Chen and Luo, 2018).

## Declaration of Competing Interest

The authors declare that they have no known competing financial interests or personal relationships that could have appeared to influence the work reported in this paper.

## Acknowledgements

This work was supported by the National Key R&D Program of China [grant number 2018YFA0605604] and the National Natural Science Foundation of China [grant number 51809243].

## References

Brubaker, K.L., Entekhabi, D., Eagleson, P.S., 1993. Estimation of Continental Precipitation Recycling. J. Clim. 6, 1077–1089. https://doi.org/10.1175/1520-0442(1993)006<1077:EOCPR>2.0.CO;2.

Castillo, R., Nieto, R., Drumond, A., Gimeno, L., 2014. The role of the ENSO cycle in the modulation of moisture transport from major oceanic moisture sources. Water Resour. Res. 50 (2), 1046–1058. https://doi.org/10.1002/2013WR013900.

Chen, Y., Luo, Y., 2018. Analysis of paths and sources of moisture for the south china rainfall during the presummer rainy season of 1979–2014. J. Meteor. Res. 32 (5), 744–757. https://doi.org/10.1007/s13351-018-8069-7.

Chen, B., Xu, X., 2016. Spatiotemporal structure of the moisture sources feeding heavy precipitation events over the Sichuan Basin. Int. J. Climatol. 36 (10), 3446–3457. https://doi.org/10.1002/joc.4567.

Chen, Y., Wang, X., Huang, L., Luo, Y., 2021. Spatial and temporal characteristics of abrupt heavy rainfall events over Southwest China during 1981–2017. Int. J. Climatol. 41 (5), 3286–3299. https://doi.org/10.1002/joc.v41.510.1002/joc.7019.

Chu, Q.-C., Zhi, R., Wang, Q.-G., Feng, G.-L., 2019. Roles of moisture sources and transport in precipitation variabilities during boreal summer over East China. Clim. Dyn. 53 (9-10), 5437–5457. https://doi.org/10.1007/s00382-019-04877-z.

Dee, D.P., Uppala, S.M., Simmons, A.J., Berrisford, P., Poli, P., Kobayashi, S., Andrae, U., Balmaseda, M.A., Balsamo, G., Bauer, P., Bechtold, P., Beljaars, A.C.M., van de Berg, L., Bidlot, J., Bormann, N., Delsol, C., Dragani, R., Fuentes, M., Geer, A.J., Haimberger, L., Healy, S.B., Hersbach, H., Hólm, E.V., Isaksen, L., Kållberg, P., Köhler, M., Matricardi, M., McNally, A.P., Monge-Sanz, B.M., Morcrette, J.-J., Park, B.-K., Peubey, C., de Rosnay, P., Tavolato, C., Thépaut, J.-N., Vitart, F., 2011. The ERA-interim reanalysis: configuration and performance of the data assimilation system. Q. J. Roy. Meteorol. Soc. 137 (656), 553–597. https://doi.org/10.1002/qj.828.

Draxler, R.R., Hess, G.D., 1997. Description of the HYSPLIT_4 Modeling System. NOAA Tech. Memo. ERL ARL–224, 24 pp.

Draxler, R.R., Hess, G.D., 1998. An overview of the HYSPLIT_4 modelling system for trajectories. Aust. Meteor. Mag. 47, 295–308.

Eagleson, P.S., 1970. Dynamic Hydrology. McGraw-Hill Inc, New York, p. 462.

Easterling, D.R., Meehl, G.A., Parmesan, C., Changnon, S.A., Karl, T.R., Mearns, L.O., 2000. Climate extremes: observations, modeling, and impacts. Science 289, 2068–2074. https://doi.org/10.1126/science.289.5487.2068.

Gaffney, S., 2004. Probabilistic curve-aligned clustering and prediction with mixture models. Ph. D. dissertation, Department of Computer Science, University of California, Irvine, 281 pp.

Hu, Q., Jiang, D., Lang, X., Yao, S., 2021. Moisture sources of summer precipitation over eastern China during 1979–2009: a lagrangian transient simulation. Int. J. Climatol. 41 (2), 1162–1178. https://doi.org/10.1002/joc.v41.210.1002/joc.6781.

Huang, Y., Cui, X., 2015. Moisture sources of torrential rainfall events in the Sichuan basin of China during summers of 2009–13. J. Hydrometeorol. 16, 1906–1917. https://doi.org/10.1175/JHM-D-14-0220.1.

Jiang, X., Li, Y., Li, C., Du, J., 2007. Characteristics of summer water vapor transportation in Sichuan Basin and its relationship with regional drought and flood (in Chinese). Plateau Meteorol. 2007, 476–484.

Jiang, X., Shu, J., Wang, X., Huang, X., Wu, Q., 2017a. The roles of convection over the Western Maritime continent and the philippine sea in interannual variability of summer rainfall over Southwest China. J. Hydrometeorol. 18, 2043–2056. https://doi.org/10.1175/JHM-D-16-0292.1.

Jiang, Z., Jiang, S., Shi, Y.i., Liu, Z., Li, W., Li, L., 2017b. Impact of moisture source variation on decadal scale changes of precipitation in North China from 1951 to 2010. J. Geophys. Res. Atmos. 122 (2), 600–613. https://doi.org/10.1002/2016JD025795.

Kalabokas, P., Jensen, N.R., Roveri, M., Hjorth, J., Eremenko, M., Cuesta, J., Dufour, G., Foret, G., Beekmann, M., 2020. A study of the influence of tropospheric subsidence on spring and summer surface ozone concentrations at the JRC Ispra station in northern Italy. Atmos. Chem. Phys. 20 (4), 1861–1885. https://doi.org/10.5194/acp-20-1861-2020.

Kim, H.C., Chai, T., Stein, A., Kondragunta, S., 2020. Inverse modeling of fire emissions constrained by smoke plume transport using HYSPLIT dispersion model and geostationary satellite observations. Atmos. Chem. Phys. 20 (17), 10259–10277. https://doi.org/10.5194/acp-20-10259-2020.

Li, D., Sun, J., Fu, S., Wei, J., Wang, S., Tian, F., 2016a. Spatiotemporal characteristics of hourly precipitation over central eastern China during the warm season of 1982–2012. Int. J. Climatol. 36 (8), 3148–3160. https://doi.org/10.1002/joc.4543.

Li, X., Zhou, W., Chen, Y.D., 2016b. Detecting the origins of moisture over southeast China: seasonal variation and heavy rainfall. Adv. Atmos. Sci. 33 (3), 319–329. https://doi.org/10.1007/s00376-015-4197-5.

Li, Y., Xu, H., Gao, Y., Li, Q., 2010. The characteristics of moisture transport associated with drought /flood in summer over the east of the southwestern China (in Chinese). Acta Meteorol. Sin. 68, 932–943.

Meseguer-Ruiz, O., Ponce-Philimon, P.I., Baltazar, A., Guijarro, J.A., Serrano-Notivoli, R., Olcina Cantos, J., Martin-Vide, J., Sarricolea, P., 2020. Synoptic attributions of extreme precipitation in the Atacama Desert (Chile). Clim. Dyn. 55 (11-12), 3431–3444. https://doi.org/10.1007/s00382-020-05455-4.

Nieto, R., Ciric, D., Vázquez, M., Liberato, M.L.R., Gimeno, L., 2019. Contribution of the main moisture sources to precipitation during extreme peak precipitation months. Adv. Water Resour. 131, 103385. https://doi.org/10.1016/j.advwatres.2019.103385.

Pathak, A., Ghosh, S., Kumar, P., 2014. Precipitation recycling in the Indian subcontinent during summer monsoon. J. Hydrometeorol. 15, 2050–2066. https://doi.org/10.1175/JHM-D-13-0172.1.

Peng, D., Zhou, T., Zhang, L., 2020. Moisture sources associated with precipitation during dry and wet seasons over Central Asia. J. Clim. 33, 10755–10771. https://doi.org/10.1175/JCLI-D-20-0029.1.

Rapolaki, R.S., Blamey, R.C., Hermes, J.C., Reason, C.J.C., 2020. Moisture sources associated with heavy rainfall over the Limpopo River Basin, southern Africa. Clim. Dyn. 55 (5-6), 1473–1487. https://doi.org/10.1007/s00382-020-05336-w.

Sodemann, H., Zubler, E., 2009. Seasonal and inter-annual variability of the moisture sources for Alpine precipitation during 1995–2002. Int. J. Climatol., 30, 947–961. https://doi.org/10.10 02/joc.1932.

Sodemann, H., Schwierz, C., Wernli, H., 2008. Interannual variability of Greenland winter precipitation sources: lagrangian moisture diagnostic and North Atlantic Oscillation influence. J. Geophys. Res. 113, D03107. https://doi.org/10.1029/2007JD008503.

Sprenger, M., Wernli, H., 2015. The LAGRANTO Lagrangian analysis tool—Version 2.0. Geosci. Model Dev. 8 (8), 2569–2586. https://doi.org/10.5194/gmd-8-2569-2015.

Stohl, A., Seibert, P., 1998. Accuracy of trajectories as determined from the conservation of meteorological tracers. Q. J. R. Meteorol. Soc. 124 (549), 1465–1484. https://doi.org/10.1002/qj.49712454907.

Stohl, A., James, P., 2004. A Lagrangian analysis of the atmospheric branch of the global water cycle. Part I: method description, validation, and demonstration for the August 2002 flooding in central Europe. J. Hydrometeor. 5, 656–678. https://doi.org/10.1175/1525-7541(2004)005<0656:ALAOTA>2.0.CO;2.

Stohl, A., James, P., 2005. A lagrangian analysis of the atmospheric branch of the global water cycle. Part II: moisture transports between Earth's ocean basins and river catchments. J. Hydrometeor. 6, 961–984. https://doi.org/10.1175/JHM470.1.

Sun, B.o., Wang, H., 2015. Analysis of the major atmospheric moisture sources affecting three sub-regions of East China. Int. J. Climatol. 35 (9), 2243–2257. https://doi.org/10.1002/joc.2015.35.issue-910.1002/joc.4145.

Sun, B., Wang, H., 2014. Moisture sources of semi-arid grassland in China using the Lagrangian particle model FLEXPART. J. Clim. 27, 2457–2474. https://doi.org/10.1175/JCLI-D-13-00517.1.

Tichý, O., Šmídl, V., Hofman, R., Šindelářová, K., Hýža, M., Stohl, A., 2017. Bayesian inverse modeling and source location of an unintended 131I release in Europe in the fall of 2011. Atmos. Chem. Phys. 17, 12677–12696. https://doi.org/10.5194/acp-17-12677-2017.

Trenberth, K., 1998. Atmospheric moisture residence times and cycling: implications for rainfall rates and climate change. Clim. Change 39, 667–694. https://doi.org/10.1023/A:1005319109110.

Trenberth, K., 1999. Atmospheric moisture recycling: role of advection and local evaporation. J. Clim. 12, 1368–1381. https://doi.org/10.1175/15200442(1999)012<1368:AMRROA>2.0.CO;2.

Wernli, H., Davies, H.C., 1997. A Lagrangian-based analysis of extratropical cyclones. I: the method and some applications. Quart. J. Roy. Meteor. Soc. 123 (538), 467–489. https://doi.org/10.1002/qj.v123:53810.1002/qj.49712353811.

Xia, J., Chen, J., Wang, G., Cheng, D., 2021. Flood control strategies for the river basin enlightened by the 2020 upper Yangtze River floods (in Chinese). Adv. Earth Sci. 36 (01), 1–8.

Yang, S., Zhang, W., Chen, B., Xu, X., Zhao, R., 2020. Remote moisture sources for 6-hour summer precipitation over the Southeastern Tibetan Plateau and its effects on precipitation intensity. Atmos. Res. 236, 14. https://doi.org/10.1016/j.atmosres.2019.104803.

Yang, X., Zhao, C., Yang, Y., Fan, H., 2021. Long-term multi-source data analysis about the characteristics of aerosol optical properties and types over Australia. Atmos. Chem. Phys. 21 (5), 3803–3825. https://doi.org/10.5194/acp-21-3803-2021.

Zhou, C., Cen, S., Li, Y., Peng, G., Yang, S., Peng, G., 2011. Precipitation variation and its impacts in Sichuan in the last 50 years (in Chinese). Acta Geograph. Sin. 66, 619–626.

Zhou, C., Li, Y., Li, W., Chen, L., 2005. Climatological characteristics of water vapor transport over eastern part of Qinghai-Xizang Plateau and its surroundings (in Chinese). Plateau Meteorol. 24, 880–888.

Zhu, Y., Yu, R., 2003. Interannual variation of summer precipitation in the west of Sichuan Basin and its relationship with large-scale circulation (in Chinese). Chin. J. Atmos. Sci. 2003, 1045–1056.